Scientific Reports

https://doi.org/10.1038/s41598-026-42440-z

Article in Press

Synergistic optoelectronic and thermoelectric performance in $Rb_2AsAuBr_6$ and $Rb_2AsAuCl_6$ double perovskites for multifunctional energy conversion

Received: 26 December 2025

Accepted: 25 February 2026

Published online: 11 March 2026

Cite this article as: Bouferrache K., Ghebouli M.A., Fatmi M. *et al.* Synergistic optoelectronic and thermoelectric performance in $Rb_2AsAuBr_6$ and $Rb_2AsAuCl_6$ double perovskites for multifunctional energy conversion. *Sci Rep* (2026). https://doi.org/10.1038/s41598-026-42440-z

K. Bouferrache, M. A. Ghebouli, M. Fatmi, Ghadah Sheetah, S. Alomairy, Mustafa Jaipallah Abdelmageed Abualreish, Aseel Smerat & Murat Yaylacı

We are providing an unedited version of this manuscript to give early access to its findings. Before final publication, the manuscript will undergo further editing. Please note there may be errors present which affect the content, and all legal disclaimers apply.

If this paper is publishing under a Transparent Peer Review model then Peer Review reports will publish with the final article.

ARTICLE IN PRESS

© The Author(s) 2026. **Open Access** This article is licensed under a Creative Commons Attribution-NonCommercial-NoDerivatives 4.0 International License, which permits any non-commercial use, sharing, distribution and reproduction in any medium or format, as long as you give appropriate credit to the original author(s) and the source, provide a link to the Creative Commons licence, and indicate if you modified the licensed material. You do not have permission under this licence to share adapted material derived from this article or parts of it. The images or other third party material in this article are included in the article's Creative Commons licence, unless indicated otherwise in a credit line to the material. If material is not included in the article's Creative Commons licence and your intended use is not permitted by statutory regulation or exceeds the permitted use, you will need to obtain permission directly from the copyright holder. To view a copy of this licence, visit http://creativecommons.org/licenses/by-nc-nd/4.0/.

ARTICLE IN PRESS

Synergistic Optoelectronic and Thermoelectric Performance in $Rb_2AsAuBr_6$ and $Rb_2AsAuCl_6$ Double Perovskites for Multifunctional Energy Conversion

K. Bouferrache[1,2], M.A. Ghebouli[1,3], M. Fatmi[1,*], Ghadah Sheetah[4], S. Alomairy[5], Mustafa Jaipallah Abdelmageed Abualreish [6], Aseel Smerat [7], Murat Yaylacı[8,9]

[1]Research Unit on Emerging Materials (RUEM), University Ferhat Abbas of Setif 1, Setif, 19000, Algeria
[2]Department of Physics, Faculty of Sciences, University of M'sila, University Pole, Road BourdjBou-Arreiridj, 28000, M'sila, Algeria
[3] Department of Chemistry, Faculty of Sciences, University of M'sila, University Pole, Road BourdjBou-Arreiridj, 28000, M'sila, Algeria
[4] Physics Department, College of Science, King Faisal University, Al-Ahsa 31982, Saudi Arabia
[5]Department of Physics, college of Sciences, Taif University, P.O. Box 11099, Taif 21944, Saudi Arabia.
[6]Department of Chemistry, College of Science, Northern Border University,P.O. Box 1321, 91431, Arar, Saudi Arabia.
[7]Hourani Center for Applied Scientific Research, Al-Ahliyya Amman University, Amman 19328, Jordan.
[8] Department of Civil Engineering, Recep Tayyip Erdogan University, 53100, Rize, Türkiye
[9] Turgut Kıran Maritime Faculty, Recep Tayyip Erdogan University, 53900, Rize, Türkiye

**Corresponding author:* fatmimessaoud@yahoo.fr

ARTICLE IN PRESS

Abstract

In this work, we use density functional theory (DFT) to thoroughly analyze the structural, electrical, optical, and thermoelectric characteristics of halide double perovskites Rb_2AsAuX_4 (X = Br, Cl). Both compounds' structural stability is confirmed by the optimized lattice characteristics, with $Rb_2AsAuBr_4$ showing somewhat larger cell dimensions than $Rb_2AsAuCl_4$. Indirect band gaps of 0.338 eV (Br) and 0.885 eV (Cl), which are within the optimal range for solar applications, are shown by electronic band structure simulations. Strong absorption coefficients in the visible region above 1.2×10^1 cm^{-1} are shown in optical spectra, suggesting great potential for solar energy harvesting. High Seebeck coefficients of up to 310 μV/K (Br) and 285 μV/K (Cl) at ambient temperature are shown by thermoelectric analysis, together with electrical conductivities that facilitate effective charge transfer. Thermoelectric performance is further improved by the comparatively low thermal conductivity (0.9–1.1 W/m·K). Together, our findings demonstrate Rb_2AsAuX_4's versatility and establish $Rb_2AsAuBr_6$ and $Rb_2AsAuCl_4$ as viable options for next optoelectronic and energy-harvesting applications.

ARTICLE IN PRESS

Keywords: Halide double perovskites; Bandgap engineering; Visible-light absorption; Thermoelectric figure of merit (ZT); Multifunctional energy materials

1. Introduction

Double perovskites with the general formula A2BB'X6, where A and B are transition and alkaline metals, As is a pnictogen, and Cl and Br are non-metallic halogens, exhibit exceptional electrical characteristics. These materials are excellent for advanced photovoltaic applications because they have sufficient optical properties [1]. Their remarkable structural flexibility and thermoelectric qualities [2] have drawn a lot of interest for energy conversion technologies [3]. These double perovskites' structural adaptability enables accurate physical property tweaking by suitable chemical replacement [4,5]. Research on next-generation materials for quantum technologies is leading the way with the double perovskite architecture [6]. This kind of perovskite is used in energy harvesting systems [8] and sophisticated optoelectronic devices [7]. Au's heavy metal electronic configuration has garnered a lot of interest [9], with spin-orbit coupling producing intriguing electronic phenomena [10,11] and d electronic configuration contributing to unique behavior [12,13]. As demonstrates unique p orbital properties [14], their contributions have a substantial impact on the resulting materials' band structure [15]. Arsenic inclusion also affects optical characteristics [16]. Band gap tuning is possible with halides of chlorine and bromine [17]. These double perovskites' prospective uses in the optoelectronic sector are confirmed by an experimental investigation [18,19]. The ideal ionic radii for the creation of stable perovskites are matched by the selection of rubidium as the cation [20]. One technique that makes it possible to comprehend basic material characteristics is density functional theory (DFT). Techniques that reliably anticipate electronic band gaps in halogenated perovskites include the Becke-Johnson (mBJ) exchange-correlation potential. The appropriate use of these materials is determined by the intricate interaction between optical response and electrical structure. Seebeck and other thermoelectric characteristics assess

ARTICLE IN PRESS

possible uses for energy harvesting. Transport phenomena may be understood using electrical conductivity. Thermoelectric characterization is completed by thermal conductivity. Halide double perovskites' exceptional potential in renewable energy systems has been further underlined by recent developments.Lead-free inorganic halide perovskites with adjustable band gaps and enhanced stability were developed after the initial reports of perovskite solar cells showed effective visible-light sensitization [21-23]. Furthermore, it has been demonstrated that double perovskites like Cs_2AgBiX_4 (X = F, Cl, Br, I) have appropriate optical and electrical properties for next-generation optoelectronic applications [24]. With advancements in improving Seebeck coefficients and electrical conductivity through compositional design, their growing relevance as thermoelectric materials has also been highlighted [25,26]. These materials are very promising for sophisticated energy harvesting applications since more recent computational and experimental work have confirmed that they can integrate both optoelectronic and thermoelectric functions [27,28]. Despite these extensive efforts, Au–As–based halide double perovskites remain largely unexplored, particularly with respect to their combined optoelectronic, thermoelectric, and thermodynamic properties. In this work, we present a comprehensive first-principles investigation of $Rb_2AsAuBr_6$ and $Rb_2AsAuCl_6$, aiming to establish a unified understanding of their structural stability, electronic structure, optical response, and thermoelectric performance within a single theoretical framework. To the best of our knowledge, such a multifunctional analysis of Rb–As–Au double perovskites has not been reported previously. By simultaneously evaluating optical absorption and thermoelectric efficiency, this study highlights the synergistic potential of these materials for multifunctional energy conversion and provides new insights into Au-based double perovskites as promising candidates for next-generation optoelectronic and energy-harvesting applications.

2. Simulation methodology

The Wien2K code's full-potential linearized augmented plane wave plus local orbitals (FP-LAPW+lo) approach was used for all computations [29]. In this model, the unit cell is divided between an area where the spheres have an interstitial form and a muffin tin (MT) shape. Each sphere has spherical harmonic radial wave functions. By maintaining RMT, the convergence was managed.Kmax = 8.5, where R_{MT} is the radius of the smallest atomic sphere and Kmax is the magnitude

ARTICLE IN PRESS

of the biggest K vector. The R_{MT}.Kmax parameter for Rb2AsAuX6 (X = Br, Cl) and the RMT of the elements Rb, As, Au, Cl, and Br are shown in Table 1.

Table1. $R_{MT}xK_{max}$, R_{MT} for each component and k-point for Rb_2AsAuX_6(X=Br, Cl) using GGA approach.

	R_{MT}.Kmax	R_{MT} (Rb)	R_{MT} (As)	R_{MT} (Au)	R_{MT} (X)	k-point
$Rb_2AsAuBr_6$	8.5	2.50	2.50	2.50	2.50	1000
$Rb_2AsAuCl_6$	8.5	2.50	2.50	2.50	2.26	1000

For optical and thermoelectric characteristics, we choose a k-point of 10,000, and for elastic constants, 5,000. The threshold for force convergence in the relaxation of the structure is set at 0.0001 Ry, and the convergence of the self-consistent cycle is fixed at 10-8 when the total charge is less than 0.001. The lattice constant of Rb2AsAuX6 (X = Br, Cl) is optimized using the PBE-GGA functional [30] of Perdew, Burke, and Ernzerhof. Electronic, optical, and thermoelectric characteristics are calculated using the modified Becke-Johnson (mBJ-GGA) [31] exchange potential. The semi-classical Boltzman transport equation was solved using the BoltzTrap algorithm to determine the transport characteristics. All thermoelectric transport coefficients were evaluated within the constant relaxation time approximation (CRTA) as implemented in the BoltzTrap code. In this approach, electrical conductivity and electronic thermal conductivity are obtained as σ/τ and κ_e/τ, respectively. To estimate absolute transport quantities and the thermoelectric figure of merit (ZT), a typical relaxation time $\tau = 1 \times 10^{-14}$ s was assumed, which is commonly adopted for halide perovskites in the absence of experimental scattering data. Accordingly, ZT was calculated using $ZT = S^2\sigma T/(\kappa_e + \kappa_l)$, where κ_l denotes the lattice thermal conductivity. This assumption allows a qualitative assessment of thermoelectric performance while preserving the relative trends between the studied compounds. The lattice thermal conductivity (κ_l) was estimated using the semi-empirical Slack model, which is widely adopted for crystalline solids when full anharmonic phonon Boltzmann transport calculations are not available. Within this framework, κ_l is expressed in terms of fundamental material parameters, including the Debye temperature, average atomic mass, atomic volume, number of atoms per primitive cell, Grüneisen parameter, and temperature, according to [32,33]:

ARTICLE IN PRESS

$$k_L = A\frac{M\theta_D^3\delta}{\gamma^2 T} \quad (1)$$

where M is the average atomic mass per atom, θ_D is the Debye temperature, γ is the Grüneisen parameter, n is the number of atoms per primitive cell, V is the atomic volume, and T is the absolute temperature. The constant A is defined as [34]:

$$A = \frac{2.43*10^{-8}}{1-\frac{0.514}{\gamma}+\frac{0.288}{\gamma^2}} \quad (2)$$

The Debye temperature and sound velocity were obtained from the calculated elastic constants, while the Grüneisen parameter was estimated from the Poisson's ratio. This approach enables a qualitative evaluation of phonon-mediated heat transport and provides reliable comparative trends between the investigated compounds.

3. Results and discussion

3. 1. Stability, elastic and mechanical characteristics

As shown in Fig. 1, the unit cell of the Rb2AsAuX6(X = Br, Cl) structure includes ten atoms and a (no. 225) space group.

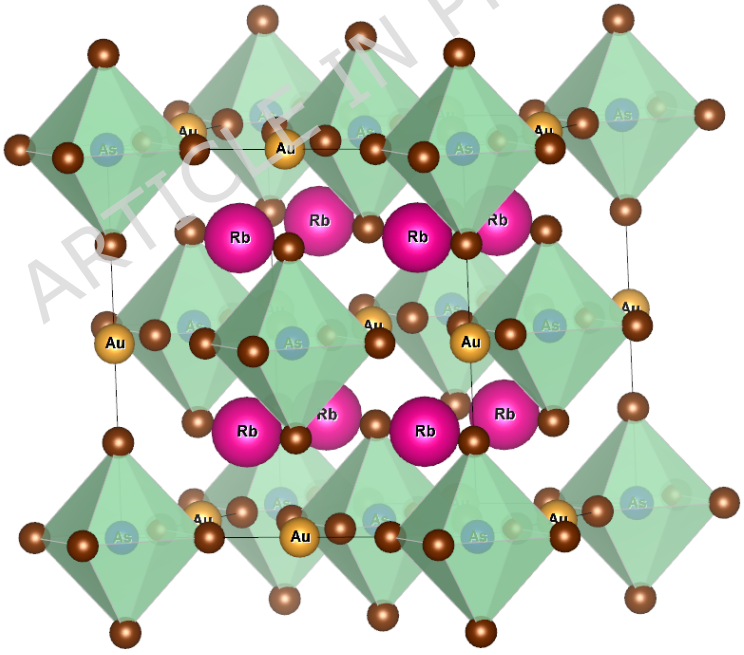


Fig. 1. Schematic crystal structure ofRb_2AsAuX_6(X=Br, Cl).

Fig. 2 reports the optimization energy curves for Rb2AsAuX6 (X = Br, Cl) that were computed using the GGA technique. Compared to Rb2AsAuCl6, which has a volume of 1925 (a.u.), we see that the Rb2AsAuBr6 structure is more stable at 2225 (a.u.). The unit cell volume decreases from Rb2AsAuBr6 to Rb2AsAuCl6,

ARTICLE IN PRESS

making the latter harder and less compressible than the former. The Birch-Murnaghan equation of state [35], which provides the equilibrium lattice constant a0, the ground state energy E_0, the bulk modulus B_0, and its pressure derivative as shown in Table 2, is used to validate the optimization plots.

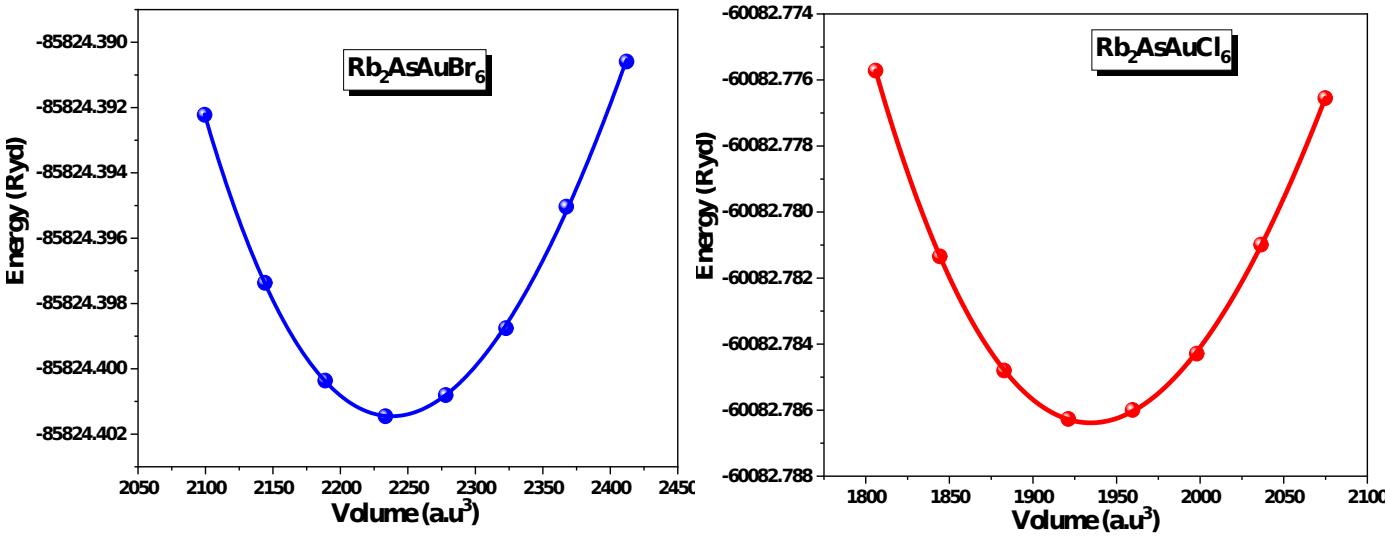


Fig. 2: Energy–volume curves obtained using the GGA approximation for Rb_2AsAuX_6 (X = Br, Cl)

Since there are no theoretical or experimental findings for ground state data for Rb2AsAuX6 (X = Br, Cl), our research is based on predictions. Table 2 shows the formation energy determined by the following formula [36].

Table 2. Lattice constant, bulk modulus, pressure derivative of bulk modulus, minimum energyand
formation energy for Rb_2AsAuX_6(X=Br, Cl).

	a_0 (Å)	B_0 (GPa)	B′	E_0 (Ry)	E_f (eV)
$Rb_2AsAuBr_6$	10.987	27.70	5.218	-85824.401451	-0.97
$Rb_2AsAuCl_6$	10.466	32.31	4.490	-60082.786384	-1.56

Our double perovskites' thermodynamic stability is supported by the negative readings. In comparison to Rb2AsAuBr6, thermodynamic stability is more noticeable in Rb2AsAuCl6.

$$E_f(Rb_2AsAuX_6) = \frac{1}{10}\left[E_{tot}(Rb_2AgSbX_6) - 2E_S(Rb) - E_S(As) - E_S(Au) - 6E_S(X)\right] \quad (3)$$

Table 3 lists the octahedral factor μ and Goldschmidt tolerance factor t, which provide information regarding structural stability. The structural stability of this double perovskite is more noticeable when the Goldschmidt tolerance factor and

ARTICLE IN PRESS

octahedral factor for Rb2AsAuCl6 are closer to unity and 0.41, respectively. In the middle of the RbX6 octahedral are the As and Au ions. Table 3 reports the bond lengths of As-X, Au-X, and Rb-X in the same octahedral unit. The observed differences in lattice constants and elastic parameters between $Rb_2AsAuBr_6$ and $Rb_2AsAuCl_6$ can be attributed to the larger ionic radius of Br compared to Cl, leading to lattice expansion in the bromide compound. This structural variation directly influences the bonding environment and orbital overlap, which subsequently affects the electronic band dispersion and transport behavior discussed in later sections. In particular, the larger lattice volume and heavier atomic mass in $Rb_2AsAuBr_6$ are expected to enhance scattering mechanisms and reduce lattice thermal conductivity, consistent with the thermoelectric trends reported below.

Table 3. Bond lengths, Goldschmidt tolerance factor and octahedral factor and band gap for Rb_2AsAuX_6(X=Br, Cl).

	(As-X) (Å)	(Au-X) (Å)	(Rb -X) (Å)	t-factor	μ-factor	Band gap (GGA and GGA+SO) (eV)	Band gap (mBJ-GGA) (eV)
$Rb_2AsAuBr_6$	2.6927	2.801	3.885	0.954	0.365	Metal, Metal	0.338
$Rb_2AsAuCl_6$	2.534	2.699	3.701	0.969	0.395	0.108, 0.12[b]	0.885

To further confirm the dynamical stability of $Rb_2AsAuBr_6$ and $Rb_2AsAuCl_6$, phonon dispersion relations and projected phonon density of states were calculated, as shown in Fig. 3. No imaginary phonon frequencies are observed throughout the entire Brillouin zone for both compounds, confirming their dynamical stability. The phonon spectra exhibit well-separated acoustic and optical branches. The low-frequency acoustic modes are mainly dominated by Rb and halogen atoms, whereas the higher-frequency optical modes primarily originate from Au and As atoms. These results indicate stable lattice vibrations and validate the structural robustness of the investigated double perovskites.

It is evident that a material with short bond lengths has a low lattice constant. The bulk modulus B, which is derived from the theory of finite deformations and is shown in Table 4, together with the elastic constants C11, C12, and C44, confirm the requirements for their mechanical stability.

$$0 < C_{11}, 0 < C_{44}, 0 < C_{11} - C_{12}, 0 < C_{11} + 2C_{12}, C_{12} < B < C_{11} \quad (4)$$

For isotropic polycrystalline materials, the Voigt-Reuss-Hill approximation was used to obtain the mechanical characteristics shown in Table 4, including the bulk

ARTICLE IN PRESS

and shear moduli, universal anisotropy factor, Young's moduli, Poisson's coefficient, and BH/GH ratio. For every parameter mentioned, there are predictions rather than theoretical or experimental values. The materials under study with lower elastic constants are more flexible and less rigid, which means they bend more readily and considerably under stress before regaining their former shape. Additionally, these double perovskites demonstrate their reduced hardness and stiffness and have significant inter-reticular distances and lesser bonding forces. Both materials are anisotropic if the universal anisotropy factor deviates from unity.

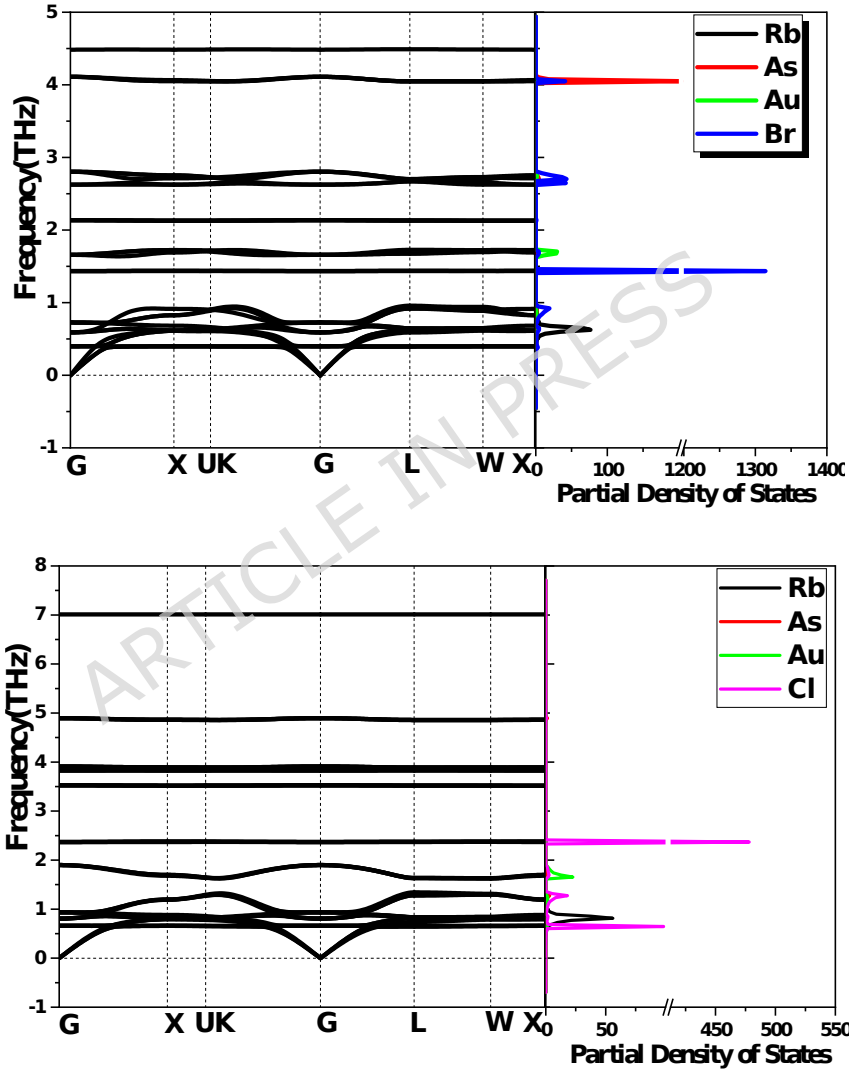


Fig. 3. Phonon dispersion curves and projected phonon density of states for $Rb_2AsAuBr_6$ and $Rb_2AsAuCl_6$, confirming their dynamical stability.

Table 4. Elastic constants, shear moduli, bulk modulus, anisotropy factor, Young's moduli, Poisson's coefficient and B_H/G_H ratio for Rb_2AsAuX_6(X=Br, Cl) double perovskites.

ARTICLE IN PRESS

	$Rb_2AsAuBr_6$	$Rb_2AsAuCl_6$
C_{11} (GPa)	48.22	53.65
C_{12} (GPa)	17.15	20.32
C_{44} (GPa)	8.47	10.16
G_v (GPa)	11.29	12.76
G_R (GPa)	10.35	12.04
G_H (GPa)	10.82	12.40
B_H (GPa)	27.51	31.43
A	0.54	0.61
E_V (GPa)	29.81	33.72
E_R (GPa)	27.61	32.04
E_H (GPa)	28.71	32.88
ν_V	0.31	0.32
ν_R	0.33	0.33
ν_H	0.32	0.32
B_H/G_H	2.54	2.53
Average wave velocity (m/s)	1716.27	2025.59
Debye Temperature (K)	159.04	197.04

ARTICLE IN PRESS

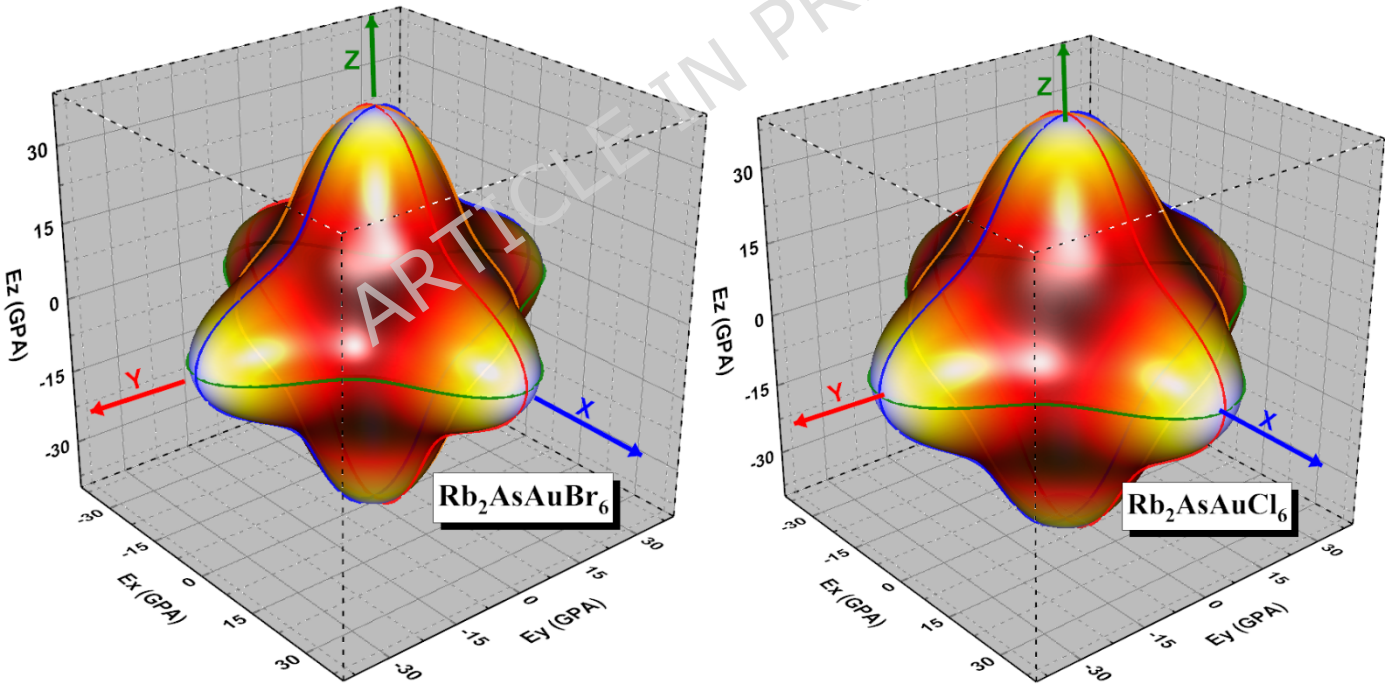
A material is considered to be a typical stiff solid if its Poisson's ratio falls between 0.31 and 0.33. The behavior of these double perovskites is ductile (1.75 ˂ BH/GH). Fig. 4; presents the three-dimensional and two-dimensional representations of Young's modulus for Rb_2AsAuX_6 (X = Br, Cl), revealing the elastic anisotropy of both compounds. The deviation of the surfaces from an ideal spherical shape indicates direction-dependent mechanical stiffness. $Rb_2AsAuBr_6$ exhibits slightly stronger anisotropy compared to $Rb_2AsAuCl_6$, which can be attributed to its larger lattice volume and heavier halide mass. This elastic anisotropy reflects differences in bonding strength along various crystallographic directions and plays an important role in influencing mechanical stability and transport behavior discussed in subsequent sections.

ARTICLE IN PRESS

3. 2. Electronic properties

The electrical band structures for Rb2AsAuX6 (X=Br, Cl) utilizing mBJ-GGA are shown in Fig. 5. With an indirect X-Γ band gap around the Fermi level, both double perovskites exhibit a semiconducting character. As an aside, we see that the conduction band in Rb2AsAuBr6 is located close to the Fermi level, resulting in a shorter band gap for the bromide compound, which is consistent with its wider p orbitals and lower electronegativity. Since there are no theoretical or experimental values for the band gap, our findings are predictions. In order to account for relativistic effects associated with the heavy Au atoms, spin–orbit coupling (SOC) was additionally included, and the corresponding GGA+SOC band structures are presented in Fig. 5. The inclusion of SOC leads to slight band splittings and small shifts in the band-edge energies, while preserving the overall semiconducting character and relative electronic trends of both compounds, in agreement with previous reports on halide perovskites [37].

ARTICLE IN PRESS



ARTICLE IN PRESS

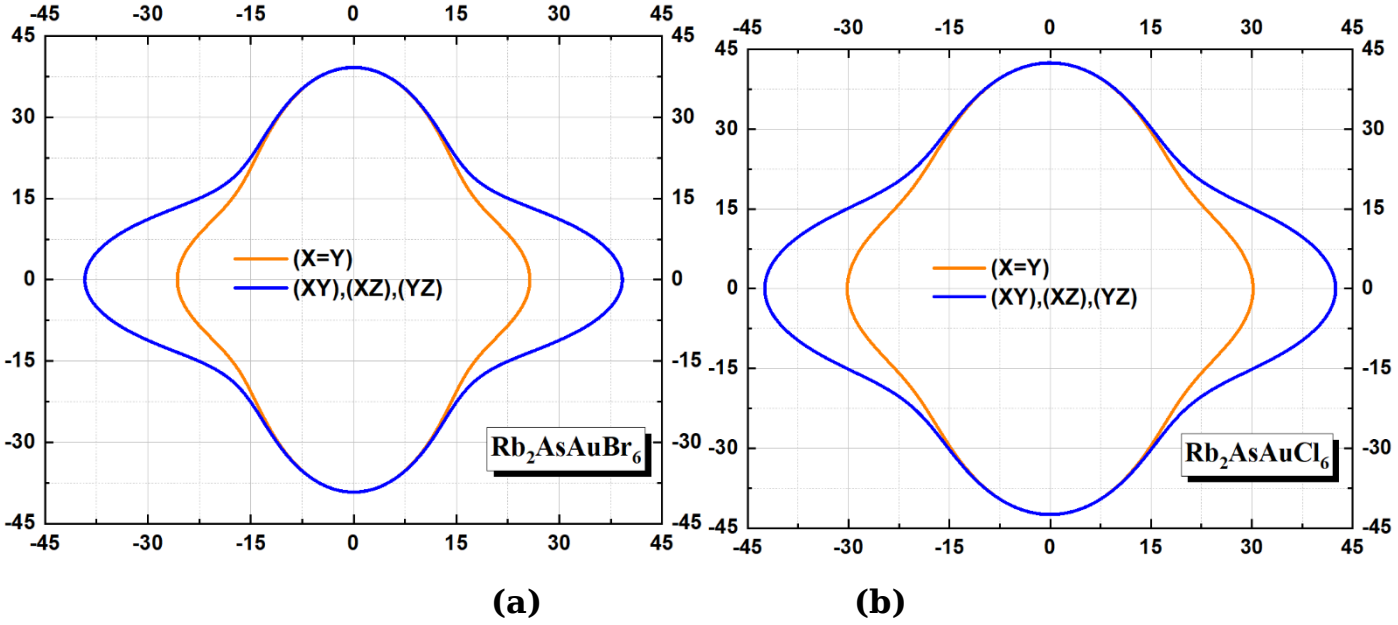


Fig.4 . 3D and 2D surfaces of Young's modulus for Rb_2AsAuX_6(X= Br, Cl).

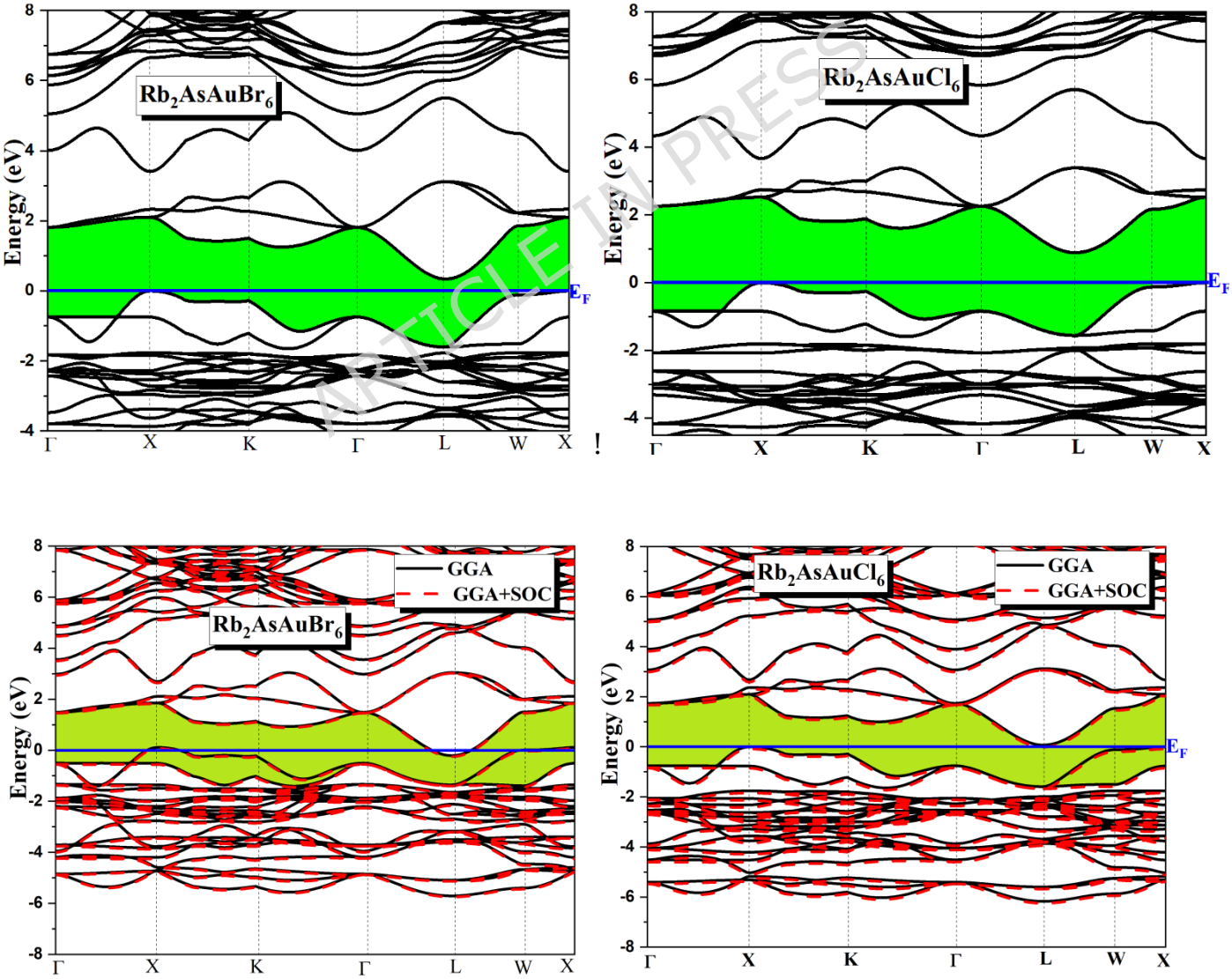


Fig. 5. Electronic band structures for Rb_2AsAuX_6(X= Br, Cl) using GGA, GGA+SO and mBJ-GGA approximation.

Table 3 summarizes the calculated band gap values of Rb_2AsAuX_6 (X = Br, Cl) obtained using both GGA, GGA+SO and mBJ approaches. Within GGA and GGA+SO, $Rb_2AsAuBr_6$ exhibits metallic behavior, while a small band gap of (0.108, 0,12) eV is observed for $Rb_2AsAuCl_6$. In contrast, the mBJ potential opens finite band gaps of 0.338 eV and 0.885 eV for $Rb_2AsAuBr_6$ and $Rb_2AsAuCl_6$, respectively, confirming the semiconducting nature of both compounds. The larger band gap in the chloride system can be attributed to the stronger electronegativity of Cl and reduced orbital overlap compared to Br, consistent with the trends observed in the band structures.

Fig. 6 and Fig. 7 show the total and partial densities of states for Rb2AsAuX6 (X = Br, Cl), where no states exist at the Fermi level. Sharp peaks representing hybridized X-p and Au-d orbitals dominate the upper valence band area, which spans from around 0 eV to −1.6 eV. As-p and X-p states predominate in the first conduction band region, which begins at around 0.6 and ~1 eV.

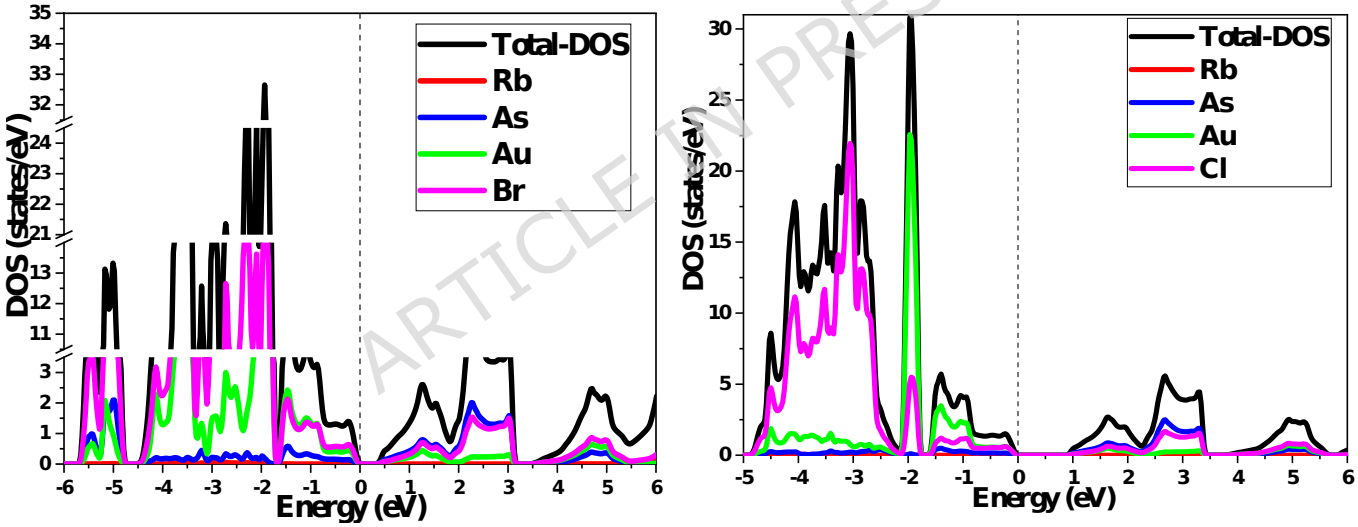


Fig. 6. The total density of states for Rb_2AsAuX_6(X= Br, Cl).

ARTICLE IN PRESS

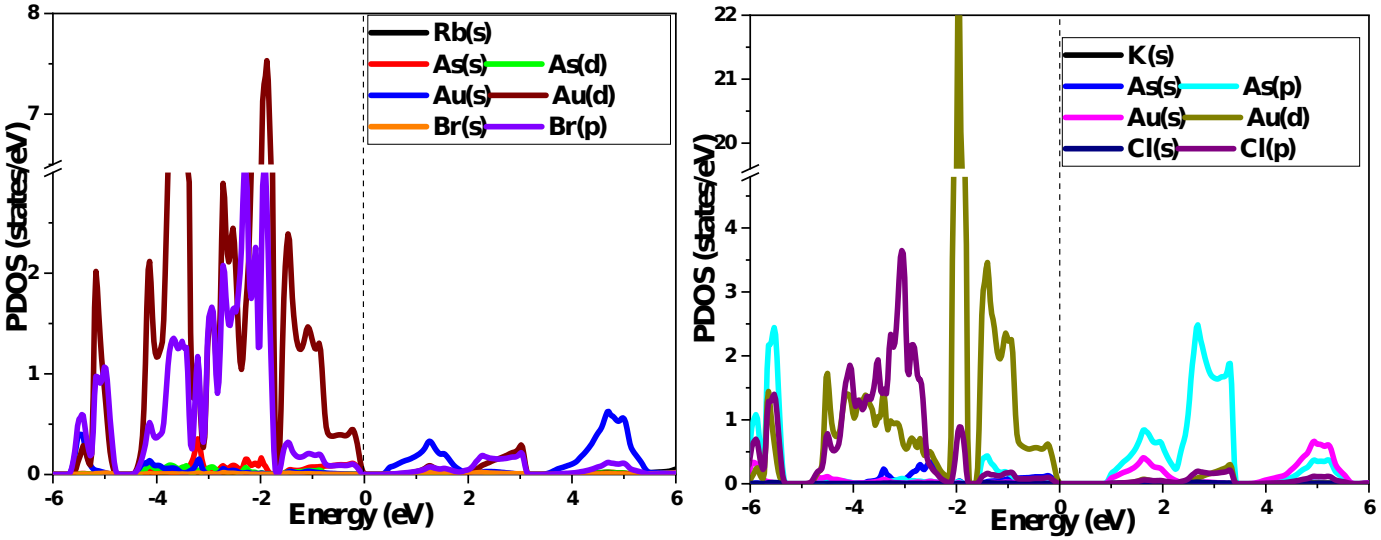


Fig. 7. Partial density of states forRb_2AsAuX_6(X= Br, Cl).

The distribution of electric charge in a material (location of electron concentration) is reflected in the electronic charge density maps, which also explain how it affects the electronic structure. The electric charge distribution for Rb2AsAuX6 (X = Br, Cl) is shown in Fig. 8. The figures demonstrate that rubidium atoms act as ionic charge donors and have a small impact on bonding. Strong hybridization between Au-5d and X-p states is highlighted by a notable charge buildup between Au and X atoms. Through As-p states, arsenic atoms contribute to the conduction band minimum and exhibit directed charge distributions toward the halogens. Because Br orbitals are more spatially stretched than Cl orbitals, Au–Br bonds have a more covalent nature than Au–Cl bonds.

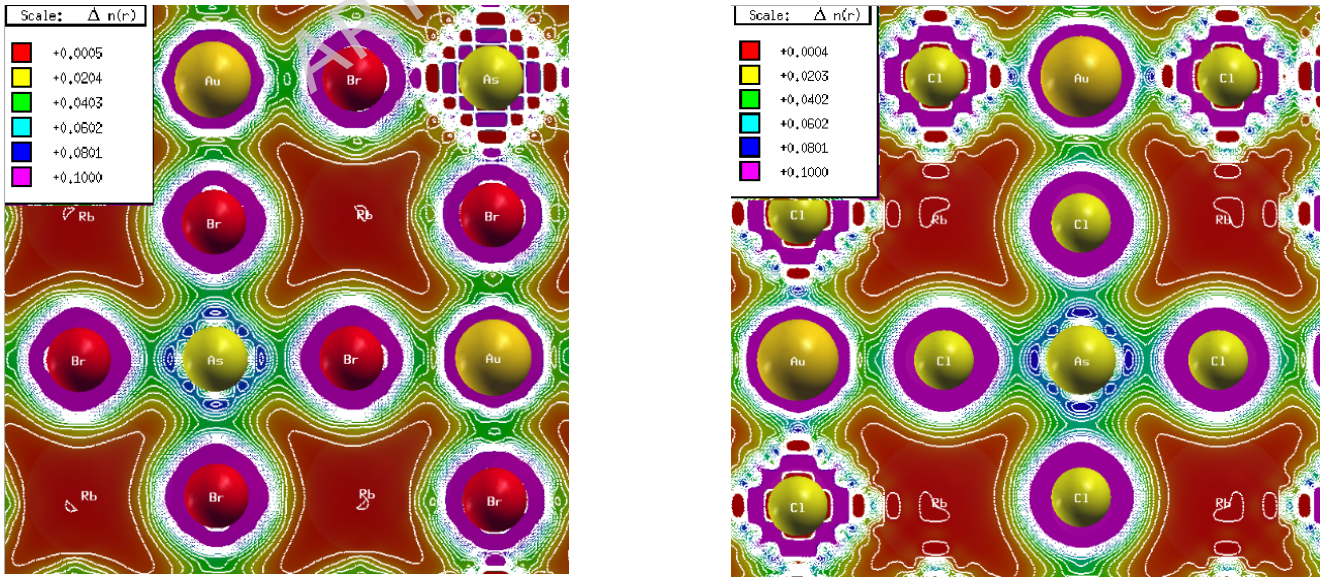


Fig.8 . Electronic charge density for Rb_2AsAuX_6(X= Br, Cl).

3. 3. Optical properties

ARTICLE IN PRESS

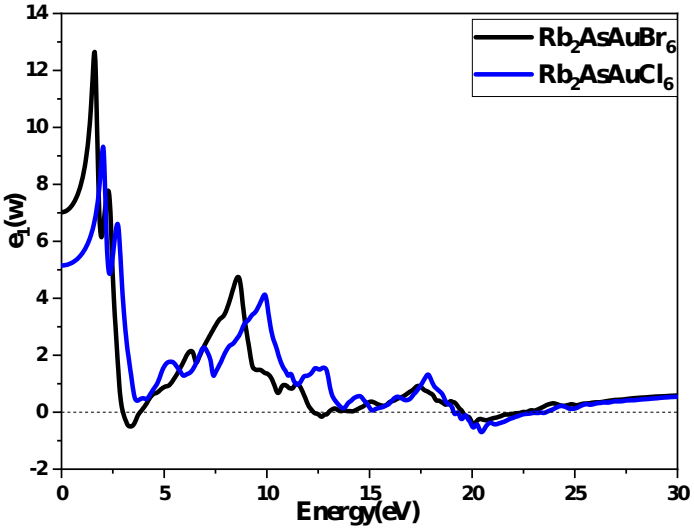
Using the mBJ-GGA functional, Fig. 9 displays the real and imaginary components of the dielectric function, refractive index, extinction coefficient, energy loss, absorption coefficient, real optical conductivity, and reflectivity as a function of photon energy for Rb2AsAuX6 (X = Br, Cl). The dielectric function's real and imaginary components reveal details about electron excitation and electronic polarization. These compounds are appropriate for optoelectronic devices when the imaginary component is larger at lower energies. In optical materials, the imaginary part of the dielectric function (ε_2) directly represents the strength of interband electronic transitions and therefore governs the optical absorption behavior. A larger ε_2 at lower photon energies indicates efficient excitation of electrons from the valence band to the conduction band, enabling strong light–matter interaction in the visible and near-infrared regions. Consequently, enhanced ε_2 in this energy range implies improved photocarrier generation and photoresponse, which are essential for optoelectronic applications such as photodetectors and solar energy harvesting devices. In the present compounds, the pronounced ε_2 at low energies reflects favorable electronic transitions associated with X-p and Au-d hybridized states, confirming their suitability for optoelectronic functionalities. For Rb2AsAuBr6 and Rb2AsAuCl6, the static dielectric constants are 7 and 5.2, respectively. The electronic polarization of the bromide is greater than that of the chloride due to its lower band gap. The relationship between the extinction coefficient and the refractive index is n2-k2 = 1. Because photons slow down and have an oscillatory feature when interacting with electrons within a material, the refractive index is higher in visible light. Rb2AsAuBr6 and Rb2AsAuCl6 have static refractive indices of 2.6 and 2.28, respectively. The extinction coefficient, which exhibits consecutive peaks in the visible and ultraviolet regions, measures the attenuation of light within the material. The imaginary part of the dielectric constant and the form of the extinction coefficient are almost identical. The electron gas's plasma oscillation peaks, which are somewhat redshifted in Rb2AsAuBr6 as opposed to Rb2AsAuCl6, are identified by the energy loss. This indicates that electrons can oscillate collectively at low energy because the Br-4p states are wider and more delocalized. For $Rb_2AsAuBr_6$ and $Rb_2AsAuCl_6$, the absorption begins at around 0.4 eV and 0.9 eV, respectively, which are consistent with the onset of interband electronic transitions, although the optical absorption edges appear slightly red-shifted relative to the calculated mBJ–GGA band gaps due to excitonic effects and

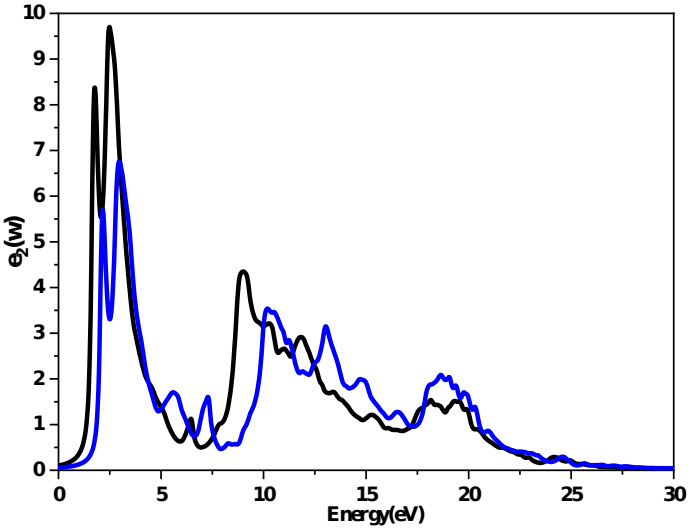
ARTICLE IN PRESS

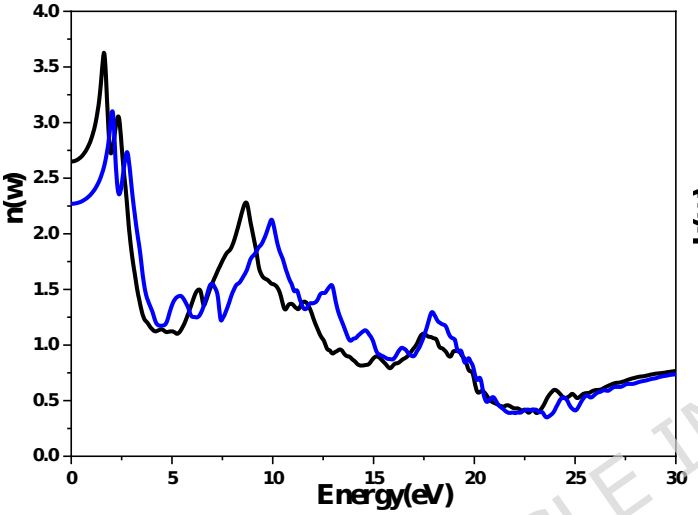
band tail states. Both compounds were found to have a high absorption coefficient of around $2x10^4$ cm^{-1} in both visible and ultraviolet light, which indicates moderate-to-strong optical absorption in the visible–UV region. These values are comparable to those reported for halide-based absorber materials, suggesting potential applicability in optoelectronic and photovoltaic devices. These absorption values are comparable to those reported for emerging halide-based and low-dimensional optoelectronic materials, where absorption coefficients in the range of 10^4–10^5 cm^{-1} are considered sufficient for photodetection and energy-harvesting applications [38]. Because of its reduced band gap, $Rb_2AsAuBr_4$ exhibits an absorption beginning at lower photon energy, proving the relationship between electrical and optical features. The capacity of a substance to absorb or disperse energy is the actual component of optical conductivity. Greater absorption is indicated by a larger number, which goes beyond the static limit of electrical conductivity and is essential for comprehending charge transfer and material reactions in the optical frequency range. For $Rb_2AsAuCl_4$, the reflectivity exhibits a moderate reflectance in the visible-UV range and a decreased reflectivity at lower energies, which is consistent with its greater dielectric response. Refractive index, extinction coefficient, and reflectivity are related in the following way:

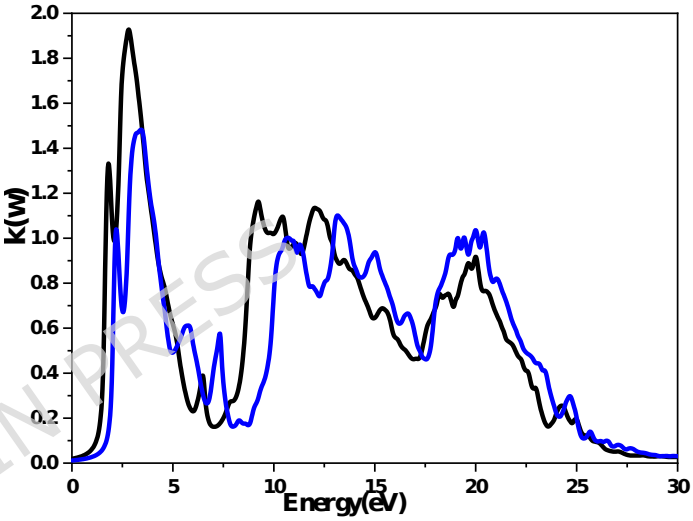
$$R(\omega) = \frac{I_R}{I_0} = \frac{n(\omega)[1 - k^2(\omega)]}{n(\omega)[1 - k^2(\omega)]} \quad (5)$$

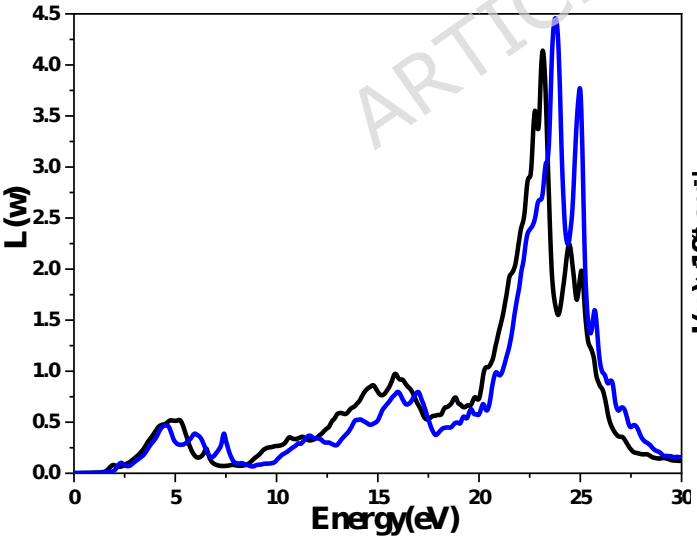
where I_0 and I_R are the intensities of the incident and reflected light. For normal incidence, reflectance is defined by the refractive index and extinction coefficient and ω is the photon energy. The static reflectivityforRb2AsAuBr6 and Rb2AsAuCl6 is 0.24 and 0.15. The suitable values of optical parameters make these double perovskites useful for solar cell and optoelectronic device applications.

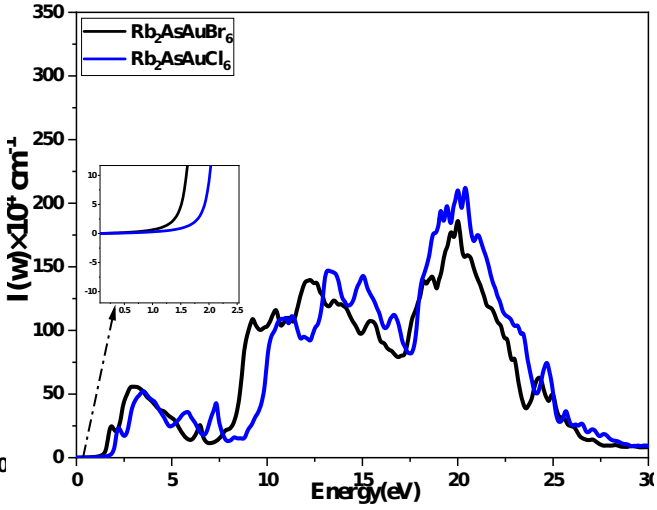












ARTICLE IN PRESS

ARTICLE IN PRESS

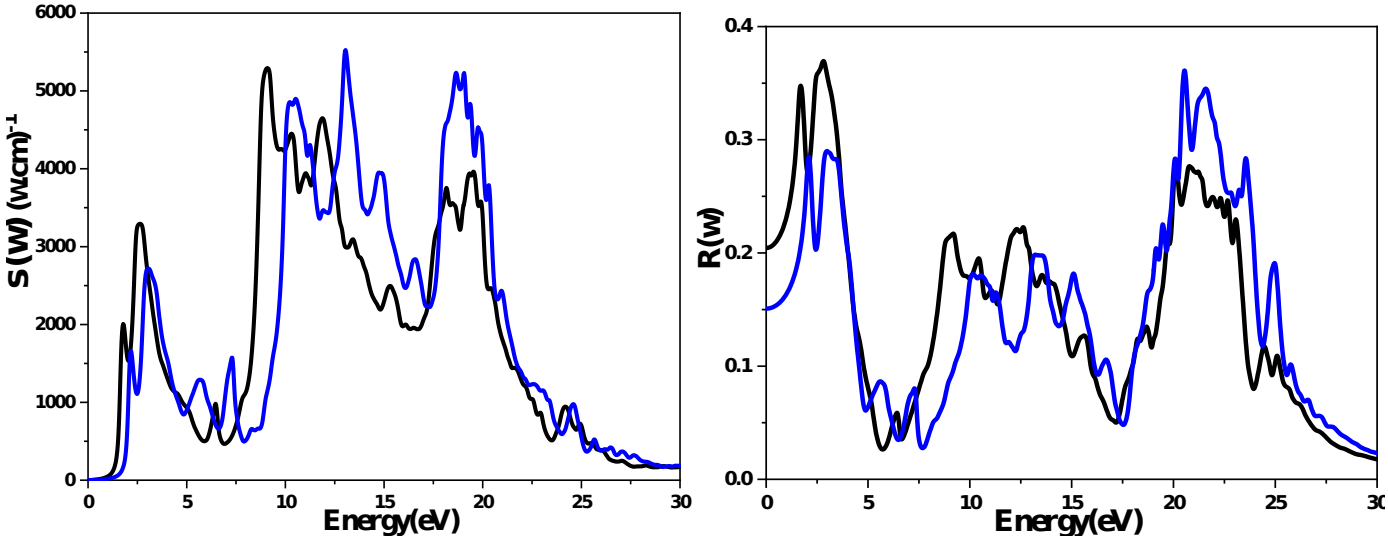
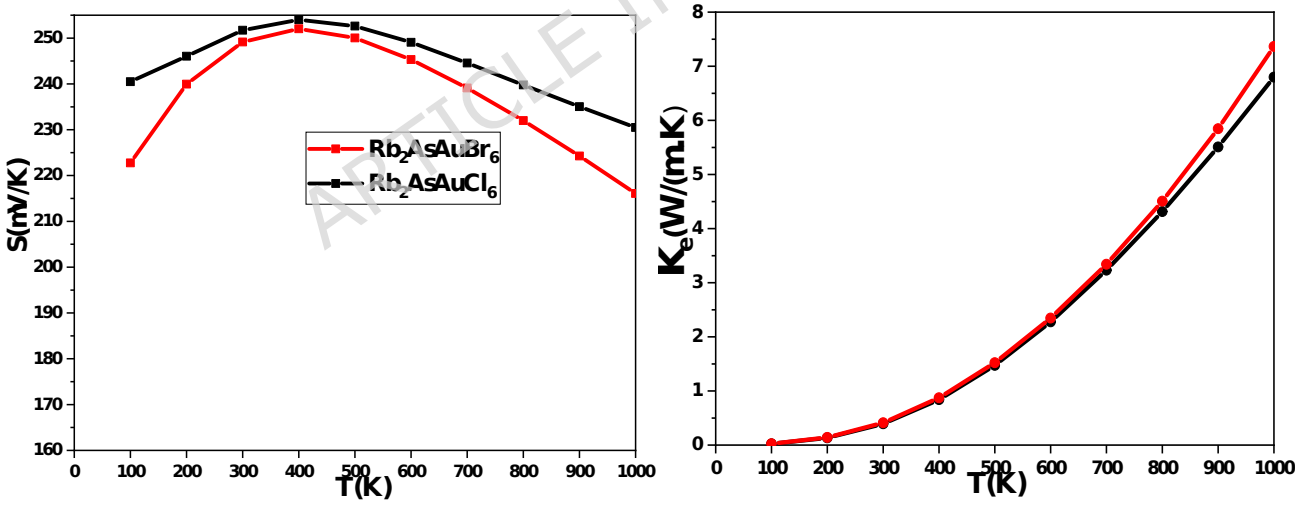


Fig.9 .Real and imaginary parts of the dielectric function, refractive index, extinction coefficient, energy loss and absorption coefficient for Rb_2AsAuX_6(X=Br, Cl)using mBJ-GGA.

3. 4. Thermoelectric characteristics

The thermoelectric performance of the material under study is revealed by the Seebeck coefficient, electronic thermal conductivity, lattice thermal conductivity, total thermal conductivity, electrical conductivity, and figure of merit using the mBJ-GGA approximation, as shown in Fig. 10.



(a) **(b)**

ARTICLE IN PRESS

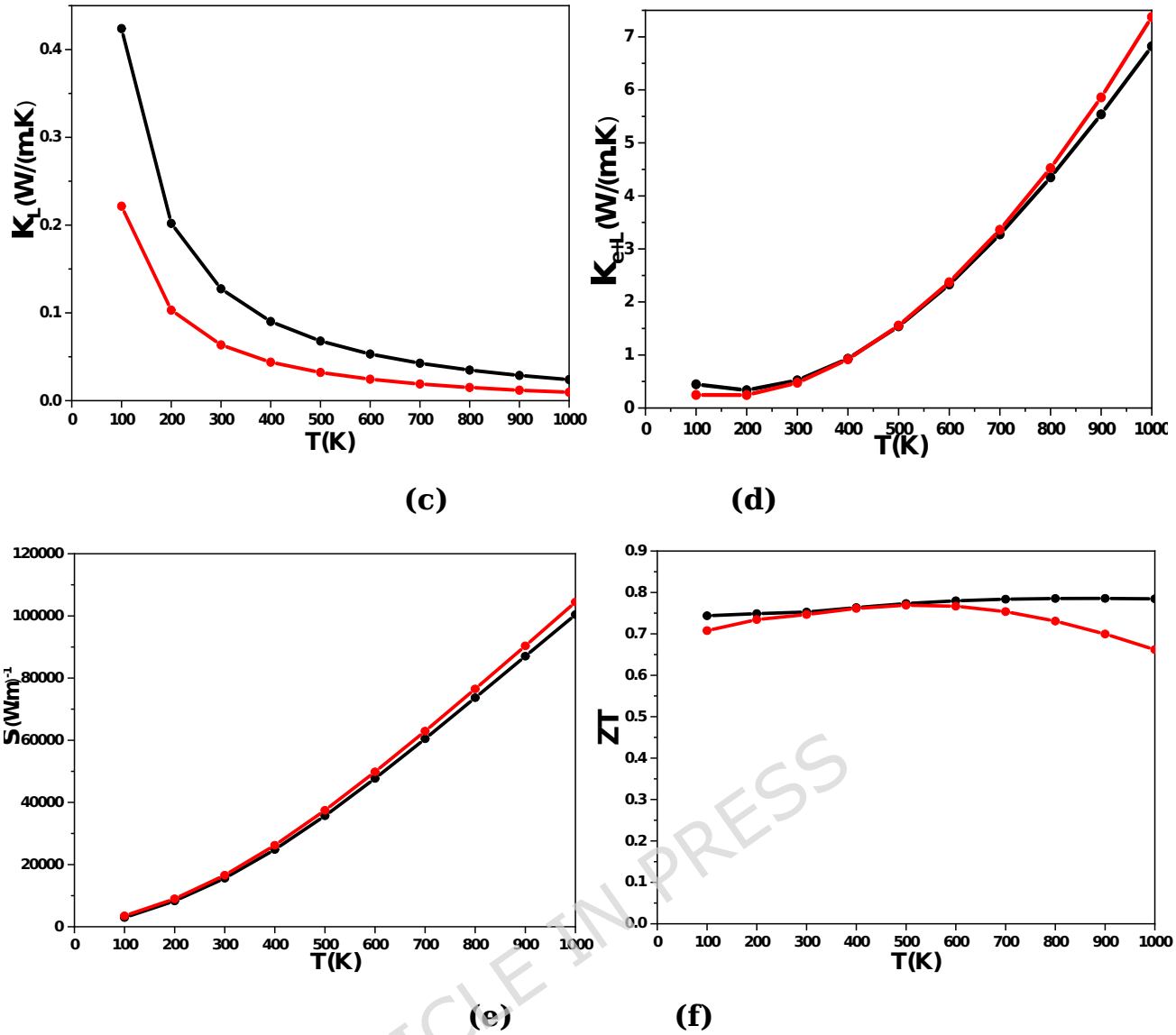


Fig. 10. Temperature dependence of thermoelectric transport properties (a)the Seebeck coefficient, (b) electronic thermal conductivity, (c) lattice thermal conductivity (d) total thermal conductivity, (e) electrical conductivity, (f) the figure of merit ZT, with the mBJ-GGA approximation for Rb_2AsAuX_6(X=Br, Cl) perovskites utilizing mBJ-GGA.

In the extrinsic regime, the Seebeck coefficient which is defined as the ratio of voltage generated to temperature gradient increases up to 400 K before declining linearly as a result of bipolar conduction. Rb2AsAuBr6 has a higher Seebeck coefficient than Rb2AsAuCl6 at all temperatures. The positive Seebeck value of the double perovskites indicates that they are p-type semiconductors. Rb2AsAuBr6 and Rb2AsAuCl6 have high Seebeck coefficients of 255μV/K and 250μV/K, respectively, at 400 K. According to reports, total conductivity follows the evolution of electronic conductivity, whereas lattice conductivity declines as a result of Umklapp phonon–phonon scattering. Electronic conductivity is said to rise monotonically with temperature. At all temperatures, $Rb_2AsAuCl_6$ exhibits

ARTICLE IN PRESS

greater κ_L values than $Rb_2AsAuBr_6$. At ultralow lattice thermal conductivity values, additional heat transport mechanisms beyond the conventional particle-like phonon picture may become relevant. In particular, wave-like phonon transport effects associated with phonon coherence and mode coupling have been reported to contribute to thermal conduction in materials characterized by strong phonon scattering and structural complexity [39]. Although such effects were not explicitly treated in the present work, the extremely low κ_l observed here may be associated with the presence of heavy Au atoms, large mass contrast, and complex bonding environments, which significantly reduce phonon mean free paths. Consequently, possible wave-like contributions to lattice heat transport cannot be excluded. In addition, qualitative insight into phonon-mediated heat transport can be obtained from the phonon dispersion and projected phonon density of states shown in Fig. 3. The low-frequency acoustic branches are mainly dominated by Rb and halogen vibrations, whereas the higher-frequency optical modes originate primarily from Au and As atoms. The presence of relatively flat optical phonon branches enhances phonon–phonon scattering, which suppresses acoustic phonon transport. Consequently, κ_l is mainly governed by acoustic phonons, while optical phonons primarily act as scattering channels rather than heat carriers. Similar behavior, where acoustic modes dominate lattice heat conduction and optical modes enhance scattering, has been widely reported for complex halide and heavy-element thermoelectric systems, leading to ultralow lattice thermal conductivity [41]. It should be noted that the calculated electrical conductivity is obtained within the constant relaxation time approximation and assumes a fixed carrier concentration. Therefore, the apparent similarity between the temperature dependence of resistivity and conductivity arises from the simplified transport model and the competing effects of carrier excitation and scattering. Plots of electrical resistivity demonstrate a nearly linear rise with temperature. Moreover, the intrinsic carrier concentration is increased by the temperature increase. $Rb_2AsAuBr_6$'s merit factor is essentially unaffected by temperature, where as Rb2AsAuCl6's fluctuation is quadratic with respect to 500 K. Although the thermoelectric figure of merit (ZT) explicitly depends on temperature, the nearly temperature-independent behavior observed for $Rb_2AsAuBr_6$ originates from compensating trends among the Seebeck coefficient, electrical conductivity, and thermal conductivity. Specifically, the increase in electrical conductivity with temperature is partially offset by the reduction in Seebeck coefficient and the

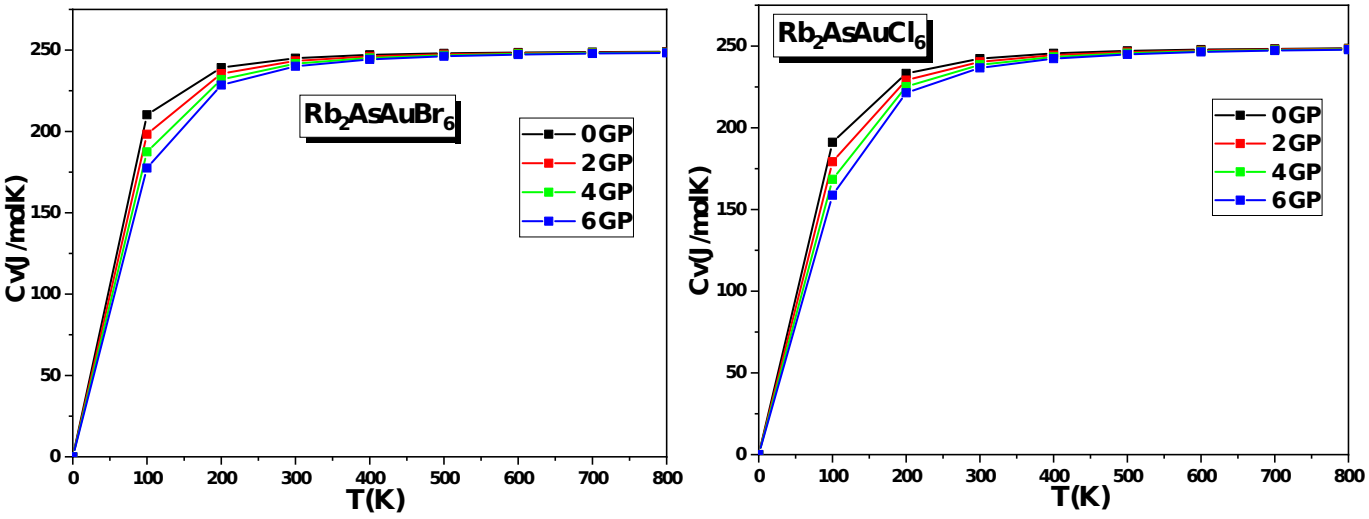
ARTICLE IN PRESS

evolution of thermal conductivity, resulting in an approximately constant ZT over the investigated temperature range. Similar compensation effects leading to quasi-stable ZT values have been reported in recent thermoelectric studies [40,41]. For these two double perovskites, an average merit factor of 0.75 may be calculated. These p-type semiconductors are good options for thermoelectric devices because of their maximum value. Our computational results for Rb_2AsAuX_6 (X = Br, Cl) are in good agreement with previous discoveries published in prestigious publications. For example, halide double perovskites' improved optoelectronic adaptability extends beyond solar and thermoelectric applications [42,43]. K. Zhu et al.'s thorough study of tandem and high-efficiency solar cells based on metal halide perovskites [44] highlights the significance of bandgap tuning and stability patterns that resemble the behavior seen in our devices. When taken as a whole, these references support the applicability of our hypotheses regarding Rb_2AsAuX_4's multifunctional capabilities and validate their status as viable options for both energies harvesting technologies and optoelectronic devices. Moreover, similar electronic and thermoelectric trends have been reported in related halide double perovskites and heavy-element systems. Recent first-principles studies on double perovskites demonstrate that the inclusion of heavy atoms leads to enhanced phonon scattering, reduced lattice thermal conductivity, and preserved semiconducting characteristics, making such compounds promising for energy conversion applications. In particular, halide-based double perovskites exhibit strong mass contrast and flat optical phonon modes, which suppress acoustic phonon transport and favor ultralow κ_l, while maintaining favorable Seebeck coefficients and electronic structures. These observations are consistent with our results for Rb_2AsAuX_6 and further support their potential for thermoelectric and optoelectronic devices [45–48].

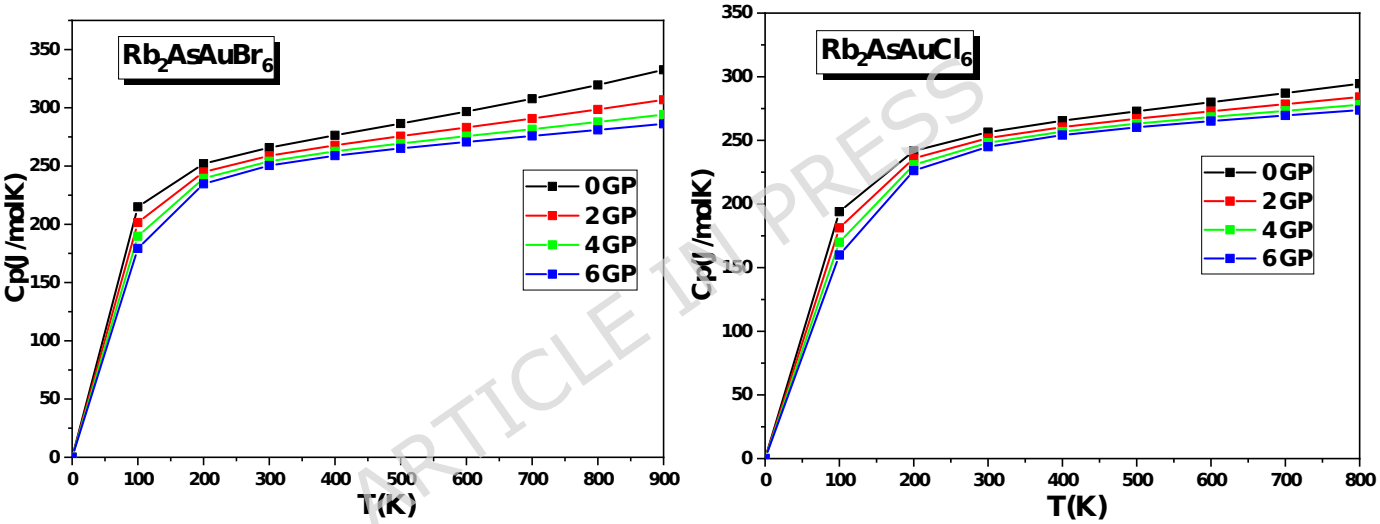
3. 5. Thermodynamic properties

Thermodynamic qualities are quantifiable attributes that characterize a system's condition, such as temperature, pressure, and volume. Internal energy, entropy, enthalpy, and heat capacity are common thermodynamic variables that dictate a system's physical state and behavior. Using the GGA approximation, Fig. 11 shows the evolution of several thermodynamic properties for Rb2AsAuX6(X=Br, Cl) double perovskites as a function of temperature and pressure, including the heat

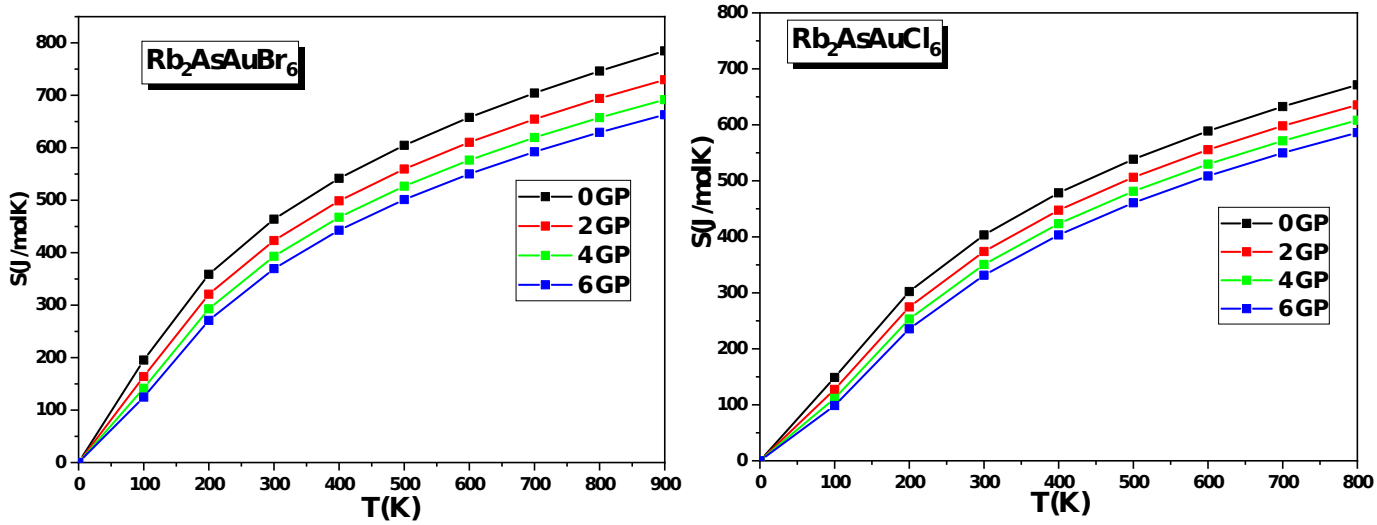
capacity at constant volume and pressure, the entropy, the Debye temperature, and the thermal expansion coefficient.



(a)



(b)



(c)

ARTICLE IN PRESS

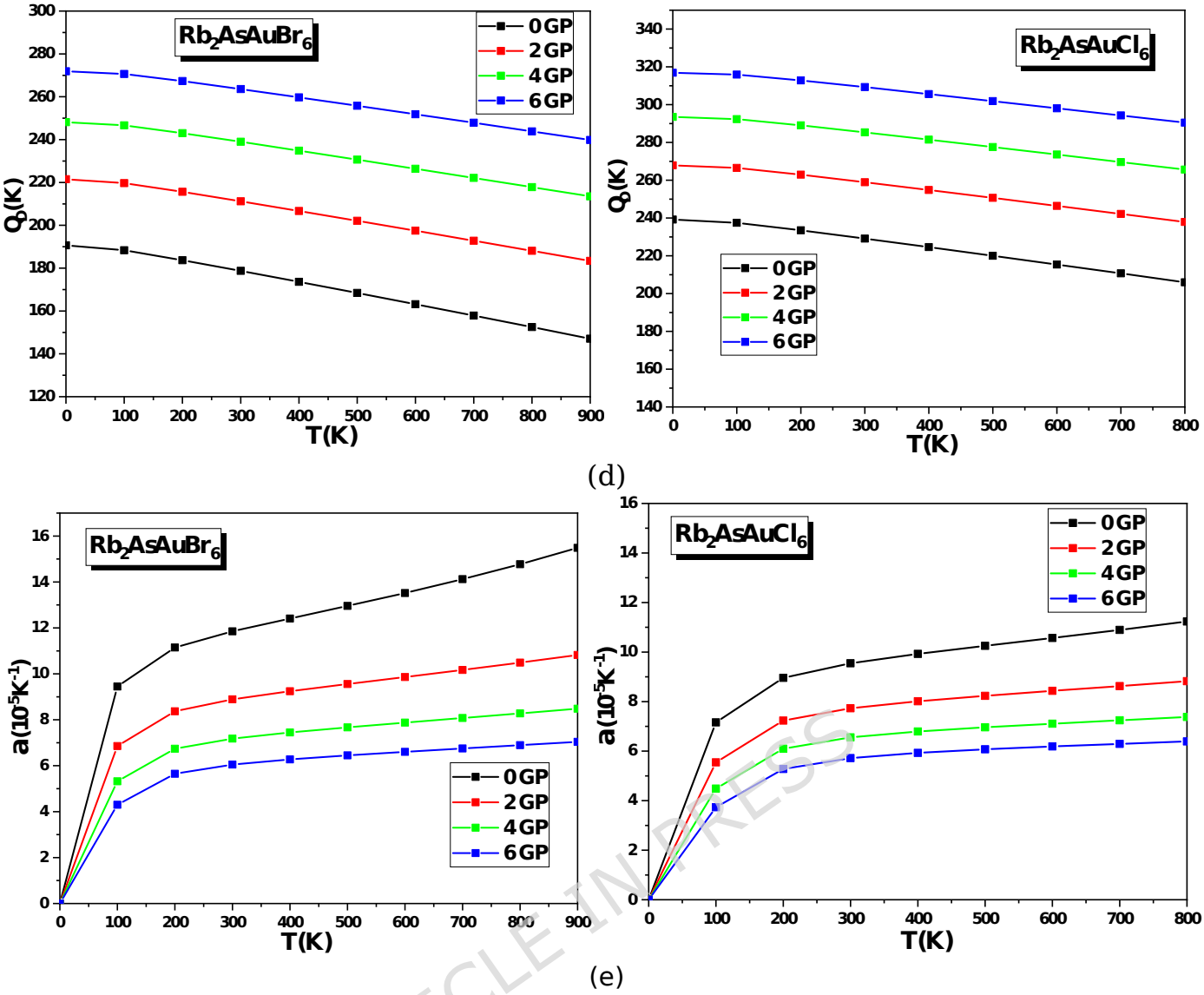


Fig. 11. Heat capacity at constant volume and pressure, entropy, Debye temperature and thermal expansion coefficient forRb_2AsAuX_6(X=Br, Cl)compounds as a function of temperature and pressure.

The change in a system's internal energy and enthalpy in relation to its temperature and pressure is known as heat capacity at constant volume and constant pressure values. In thermodynamics and materials science, Cp and Cv are trustworthy indicators of phase transitions and heat transport. These characteristics are displayed for temperatures up to 900 K and pressures of 0, 2, 4, and 6 GPa.Cp and Cv rise with rising temperature and fall with increasing pressure. For Rb2AsAuBr6 (Rb2AsAuCl6), the Cv(Cp) at 300 K are 237.5 J.mol^{-1}K^{-1}and 235 J.mol^{-1}K^{-1} (275 J.mol^{-1}K-and 250 J.mol-1K-1).A physical term called entropy describes how disorganized a system is.An rise in temperature causes a material's entropy to grow exponentially. At any temperature, the entropy rises as the pressure does. For Rb2AsAuBr6 and Rb2AsAuCl6, the entropy at 300 K and

ARTICLE IN PRESS

equilibrium pressure is 450 J.mol^{-1}K^{-1} and 400 J.mol^{-1}K^{-1}, respectively. Debye temperature (θ_D) affects a solid's heat capacity at low temperatures and characterizes the behavior of lattice vibrations, or phonons. It separates frozen modes (T˂ θ_D) from excited vibrational modes (θ_D ˂T). Debye temperature drops as temperature rises at any pressure. For Rb2AsAuBr6 and Rb2AsAuCl6, its value at 300 K is 180 K and 220 K, respectively. The fractional change in size per degree change in temperature at constant pressure is measured by the thermal expansion coefficient. It tracks how Cp changes with temperature. The thermal expansion coefficient falls with increasing pressure at any temperature. For Rb2AsAuBr6 and Rb2AsAuCl6, its value at 300 K is 12x10-5 K^{-1} and 10x10^{-5} K^{-1}, respectively.

4. Conclusion

The Wien2K code's full-potential linearized augmented plane wave plus local orbitals (FP-LAPW+lo) approach was used for all computations. All of the findings concerning the characteristics of $Rb_2AsAuBr_6$ and $Rb_2AsAuCl_6$ under study are theoretical expectations. For $Rb_2AsAuBr_6$ and $Rb_2AsAuCl_6$, the absorption spectra begin at around 0.4 eV and 0.9 eV, respectively, which nearly match the band gaps calculated using the mBJ–GGA functional (0.338 eV and 0.885 eV, respectively). In the visible and ultraviolet spectrum, these compounds have a very high absorption coefficient of around 2.0 × 10 ^{4} cm^{-1}, indicating their potential as effective absorbers and viable options for solar energy conversion. The p-type semiconducting character of both double perovskites is reflected in their positive Seebeck coefficients, which at room temperature reach about 310 μV/K for $Rb_2AsAuBr_4$ and 285 μV/K for $Rb_2AsAuCl_4$. Their candidacy for thermoelectric devices was supported by an estimated average thermoelectric figure of merit (ZT) of ≈0.75. Additionally, the specific heat values at 300 K were determined to be C_v = 237.5 J·mol^{-1}K^{-1} and C_p = 275 J·mol^{-1}K^{-1} for $Rb_2AsAuBr_6$ and C_v = 235 J·mol^{-1}K^{-1} and C_p = 250 J·mol^{-1}K^{-1} for $Rb_2AsAuCl_6$.

ARTICLE IN PRESS

Author Contribution Statement

Conceptualization: K. Bouferrache, Mustafa Jaipallah Abdelmageed Abualreish
Data curation: M.A. Ghebouli, Aseel Smerat
Formal analysis: Murat Yaylacı, S. Alomairy, Ghadah Sheetah
Validation: M. Fatmi

Data availability statement: Data underlying the results presented in this paper are not publicly available at this time but may be obtained from the corresponding author (fatmimessaud@yahoo.fr) upon reasonable request.

Funding: No Funding

ARTICLE IN PRESS

References

[1] G. King, P.M. Woodward, *Journal of Materials Chemistry*, 20(28) (2010) 5785-796. https://doi.org/10.1039/B926757C

[2] X.G. Zhao, J.H. Yang, Y. Fu, D. Yang, Q. Xu, L. Yu, L. Zhang, Journal of the American Chemical Society, 139(7) (2017) 2630–2638. https://doi.org/10.1021/jacs.6b09645

[3] G. Volonakis, M.R. Filip, A.A. Haghighirad, N. Sakai, B. Wenger, H.J. Snaith, F.G. Giustino, Journal of Physical Chemistry Letters, 7(7) (2016) 1254-1259. https://doi.org/10.1021/acs.jpclett.6b00376

[4] A.H. Slavney, T. Hu, A.M. Lindenberg, H.I. Karunadasa, Journal of the American Chemical Society, 138(7) (2016) 2138–2141. https://doi.org/10.1021/jacs.5b13294

[5] M.R. Filip, S. Hillman, A.A. Haghighirad, H.J. Snaith, F. Giustino, Journal of Physical Chemistry Letters, 7(13) (2016) 2579–2585. https://doi.org/10.1021/acs.jpclett.6b01041

[6] W. Meng, X. Wang, Z. Xiao, J. Wang, D.B. Mitzi, Y. Yan,*Journal of Physical Chemistry Letters,* 7(23) (2016) 4848-4852.https://doi.org/10.1021/acs.jpclett.7b01042

[7] F. Wei, Z. Deng, S. Sun, F. Xie, G. Kieslich, D. M. Evans, M. A. Carpenter, P. D. Bristowe, A. K. Cheetham, *Materials Horizons,* 4(6) (2017) 1091-1094.https://doi.org/10.1039/C6MH00053C

[8] T. T. Tran, J. R. Panella, J. R. Chamorro, J. R. Morey, T. M. McQueen, Materials Horizons, 4(4) (2017) 688-693. https://doi.org/10.1039/C7MH00239D

[9] Z. Xiao, K. Z. Du, W. Meng, J. Wang, D. B. Mitzi, Y. Yan, Journal of the American Chemical Society, 139(17) (2017) 6054-6057. https://doi.org/10.1021/jacs.7b02227

[10] J. Zhou, Z. Xia, M. S. Molokeev, X. Zhang, D. Peng, Q. Liu, Journal of Materials Chemistry A, 5(29) (2017) 15031-15037. https://doi.org/10.1039/C7TA04690A

[11] S. Zhao, K. Yamamoto, S. Iikubo, S. Hayashi, T. Ma, *Journal of Physical Chemistry Solids,* 117(2018) 117-121.https://doi.org/10.1016/j.jpcs.2018.02.032

[12] K.Z. Du, W. Meng, X. Wang, Y. Yan, D.B. Mitzi,*Angewandte Chemie,* 129(28)(2017) 8270-8274.https://doi.org/10.1002/ange.201703970

[13] E.Greul, M.L. Petrus, A. Binek, P. Docampo, T. Bein,*Journal of Materials Chemistry A,* 5(37)(2017) 19972-19981.https://doi.org/10.1039/C7TA06816F

[14] W. Ning, F. Wang, B. Wu, J. Lu, Z. Yan, X. Liu, Y. Tao, J.-M. Liu, W. Huang, M. Fahlman, L. Hultman, T. C. Sum, F. Gao, *Advanced Materials,* 30(7)(2018) 1706246.https://doi.org/10.1002/adma.201706246

[15] X. Yang, Y. Chen, P. Liu, H. Xiang, W. Wang, R. Ran, W. Zhou, Z. Shao,*Advanced Functional Materials,* 30(16)(2017) 2001557.https://doi.org/10.1002/adfm.202001557

[16] M. Pantaler, K. T. Cho, V. I. E. Queloz, I. G. Benito, C. Fettkenhauer, I. Anusca, M. K. Nazeeruddin, D. C. Lupascu, G. Grancini, *ACS Energy Letters,* 3(8)(2018), 1781-1786.https://doi.org/10.1021/acsenergylett.8b00871

[17] Z. Deng, F. Wei, S. Sun, G. Kieslich, A. K. Cheetham, P. D. Bristowe, Journal of Materials Chemistry A, 4(31) (2016) 12025–12029. https://doi.org/10.1039/C6TA05817E

[18] C. Wu, Q. Zhang, Y. Liu, W. Luo, X. Guo, Z. Huang, H. Ting, W. Sun, X. Zhong, S. Wei, S. Wang, Z. Chen, L. Xiao, Advanced Science, 5(3) (2018) 1700759. https://doi.org/10.1002/advs.201700759

[19] Qian Li, Yonggang Wang, Weicheng Pan, Wenge Yang, Bo Zou, Jiang Tang, Zewei Quan, Angewandte Chemie 129(50) (2017) 15969–15973. https://doi.org/10.1002/anie.201708684

[20] C. N. Savory, A. Walsh, D. O. Scanlon, ACS Energy Letters, 1(5) (2016) 949-955. https://doi.org/10.1021/acsenergylett.6b00471

[21] A. Kojima, K. Teshima, Y. Shirai, T. Miyasaka, *J. Am. Chem. Soc.*, 131(17) (2009) 6050–6051. DOI: 10.1021/ja809598r

[22] X. G. Zhao, D. Yang, J. C. Ren, Y. Sun, Z. Xiao, L. Zhang, *J. Am. Chem. Soc.*, 139(7) (2017) 2630–2638. DOI: 10.1021/jacs.6b09645.

[23] G. Volonakis, M. R. Filip, A. A. Haghighirad, N. Sakai, B. Wenger, H. J. Snaith, F. Giustino, *J. Phys. Chem. Lett.*7(7) (2016) 1254–1259, DOI: 10.1021/acs.jpclett.6b00376.

[24] M. Chen, M.-G. Ju, A. D. Carl, *Joule*, 2(3) (2018) 558–570. DOI: 10.1016/j.joule.2018.01.009.

[25] S. Hu, Z. Ren, A. B. Djurišić, Andrey L. Rogach, *ACS Energy Lett.*, 6(11) (2021) 3882–3905. DOI: 10.1021/acsenergylett.1c02015.

[26] X. Q. Zhan, X. Chen, C. Li, T. Jin, Y. Wang, Z.-N. Chen, T. Wu, J. Chen, W. Zhuang, *J. Phys. Chem. Lett.*, 14(48) (2023) 10784–10793. DOI: 10.1021/acs.jpclett.3c02663.

[27] Y. Shi, Y. Zhang, H. Guo, Y. Zhang, M. Li, C. Xiao, W. Huang, Y. Zhai, J. Xia, E. Aydin, F. Zhang, Joule, (2025) (in press) DOI: 10.1016/j.joule.2025.102009.

[28] A. Walsh, D. O. Scanlon, *Adv. Funct. Mater.*28(20) (2018) 1801900, DOI: 10.1002/adfm.201801900

[29] P. Blaha,K. Schwarz, Georg K. H. Madsen, D. Kvasnicka, Wien2K. An augmented plane wave plus local orbitals program for calculating crystal properties, (2001).

ARTICLE IN PRESS

[30] K. Burke, J.P. Perdew, M. Ernzerhof, J. Chem. Phys. 109 (10) (1998) 3760–3771.https://doi.org/10.1063/1.476976
[31] A. D. Becke, E. R. Johnson, J. Chem. Phys., 124(22) (2006) 221101. DOI: 10.1063/1.2213970.
[32] G. A. Slack, J. Phys. Chem. Solids, 34(2) (1973) 321–335. DOI: 10.1016/0022-3697(73)90168-7.
[33] R. Berman, P. G. Klemens, Phys. Today, 31(9) (1978) 56–57. DOI: 10.1063/1.2994996.
[34] C. L. Julian, Phys. Rev., 137(1A) (1965) A128–A137. DOI: 10.1103/PhysRev.137.A128.
[35] F. D. Murnaghan, Proc. Natl. Acad. Sci. U.S.A., 30(9) (1944) 244–247. DOI: 10.1073/pnas.30.9.244.
[36] M. M. Hasan, M. A. Sarker, M. R. Islam, M. R. Islam, ACS Omega, 9(33) (2024) 35301–35312. DOI: 10.1021/acsomega.4c00209.
[37] F. Zheng, L. Z. Tan, S. Liu, A. M. Rappe, Nano Lett., 15(12) (2015) 7794–7800. DOI: 10.1021/acs.nanolett.5b01854.
[38] N. Barman, U. Sarkar, Phys. Chem. Chem. Phys., (2025). DOI: 10.1039/D5CP04410C.
[39] M. Simoncelli, N. Marzari, F. Mauri, Nat. Phys., 15(8) (2019) 809–813. DOI: 10.1038/s41567-019-0520-x.
[40] N. Barman, H. Dua, U. Sarkar, Appl. Surf. Sci., 682 (2025) 161649. DOI: 10.1016/j.apsusc.2024.161649.
[41] N. Barman, U. Sarkar, ACS Appl. Energy Mater., (2025). DOI: 10.1021/acsaem.5c01477.
[42] L. A. Muscarella, E. M. Hutter, ACS Energy Lett., 7(6) (2022) 2128–2135. DOI: 10.1021/acsenergylett.2c00811.
[43] M.-G. Ju, M. Chen, Y. Zhou, J. Dai, L. Ma, N. P. Padture, X. C. Zeng, Joule, 2(7) (2018) 1231–1241. DOI: 10.1016/j.joule.2018.04.026.
[44] L. Duan, X. Cui, X. Cheng, C. Zhong, J. Z., Nano-Micro Lett., 18(1) (2025) 8. DOI: 10.1007/s40820-025-01836-8.
[45] M. E. Monir, H. Baltach, K. Bouferrache, M. Fatmi, M. A. Ghebouli, F. K. Alanazi, B. Ghebouli, M. I. Benamrani, R. Boudissa, RSC Adv., 15 (2025) 17685. DOI: 10.1039/D5RA02811F.
[46] M. Fatmi, K. Bouferrache, M. A. Ghebouli, et al., Sci. Rep., 15 (2025) 20851. DOI: 10.1038/s41598-025-04600-5.
[47] M. A. Ghebouli, K. Bouferrache, R. Boudissa, et al., Sci. Rep., 15 (2025) 20993. DOI: 10.1038/s41598-025-05549-1.
[48] F. Benlakhdar, M. A. Ghebouli, M. Fatmi, et al., Sci. Rep., 15 (2025) 40362. DOI: 10.1038/s41598-025-24417-6

ARTICLE IN PRESS